

Research article

**STRESS-FREE STATE OF THE RED BLOOD CELL MEMBRANE
AND THE DEFORMATION OF ITS SKELETON #**TJAŠA ŠVELC^{1*} and SAŠA SVETINA^{1,2}¹Institute of Biophysics, Faculty of Medicine, University of Ljubljana, Slovenia,²Jožef Stefan Institute, Ljubljana, Slovenia

Abstract: The response of a red blood cell (RBC) to deformation depends on its membrane, a composite of a lipid bilayer and a skeleton, which is a closed, two-dimensional network of spectrin tetramers as its bonds. The deformation of the skeleton and its lateral redistribution are studied in terms of the RBC resting state for a fixed geometry of the RBC, partially aspirated into a micropipette. The geometry of the RBC skeleton in its initial state is taken to be either two concentric circles, a references biconcave shape or a sphere. It is assumed that in its initial state the skeleton is distributed laterally in a homogeneous manner with its bonds either unstressed, presenting its stress-free state, or prestressed. The lateral distribution was calculated using a variational calculation. It was assumed that the spectrin tetramer bonds exhibit a linear elasticity. The results showed a significant effect of the initial skeleton geometry on its lateral distribution in the deformed state. The proposed model is used to analyze the measurements of skeleton extension ratios by the method of applying two modes of RBC micropipette aspiration.

Key words: Red blood cell, Stress-free shape, Membrane skeleton, Skeleton deformation, Spectrin, Micropipette aspiration

INTRODUCTION

The membrane of a red blood cell (RBC) is a composite of a bilayer and an underlying network of proteins called the membrane skeleton (below we use the term skeleton). The bilayer, which includes the transmembrane proteins embedded in a lipid matrix, behaves as an almost incompressible, two-

Paper authored by participant of the international conference: 18th Meeting, European Association for Red Cell Research, Wrocław – Piechowice, Poland, May 12-15th, 2011. Publication cost was covered by the organizers of this meeting.

* Author for correspondence. e-mail: tjasa.svelc@mf.uni-lj.si, tel.: +386 1 5437600, fax: +386 1 5437601

Abbreviation used: RBC – red blood cell

dimensional liquid, whereas the skeleton, a two-dimensional, quasi-triangular network, is elastically much softer. It is generally agreed that the bilayer provides the capacity for RBC membrane bending and the skeleton gives it its shear elasticity [1]. The mechanical deformation of the cell causes the bilayer to change its shape and the skeleton to redistribute in the plane of the membrane [2, 3]. The skeleton redistribution depends on the initial conditions, i.e., on the resting state of the RBC. The initial state of the RBC spectrin skeleton can be defined by assuming that for the prescribed cell shape it is distributed laterally in a homogeneous manner. The establishment of a homogeneous distribution of the skeleton bonds can be understood on the basis of a permanently occurring dissociation of the spectrin tetramers into dimers and their re-association, driving the system into a state of maximum entropy. The shape of the RBC membrane when it is in the stress-free state is still the subject of speculations and discussions. Different conclusions and assumptions about whether in the resting state the cell is a biconcave disc [4-6] or a sphere [7] were, e.g., summarized by Fischer *et al.* [8], who suggested that the biconcave shape is a more natural choice for the resting shape of the RBC membrane than a sphere. However, what exactly is the more appropriate reference shape of the RBC skeleton still remains controversial [9].

A possible direction to study whether the resting shape is a biconcave disc or a sphere is to observe the skeleton extension ratios. An original method for measuring the skeleton deformation was introduced by Lee *et al.* [10]. They labeled the membrane F-actin using rhodamine phalloidin and employed a “two-micropipette approach,” schematically shown in Figs. 1A and B. After a cell was aspirated into a micropipette, a part of the aspirated skeleton was marked by bleaching (Fig. 1A). The cell was then aspirated with another micropipette, placed in the opposite direction to the first micropipette (Fig. 1B). The skeleton deformation was then obtained from a comparison of the widths of the marked skeleton. A comparison of the measured extensions of the skeleton with the simulated extensions can lead to a better understanding of the resting state of an RBC. The initial state of the skeleton used in the simulation by Lee *et al.* [10] was a sphere, which they claimed was a close approximation to the true discocytic reference.

Here, we re-examine the skeleton redistribution by employing different resting shapes of the RBC. Three possible geometrical shapes were assumed as initial shapes of the RBC skeleton (Fig. 1C). In the first case the initial shape of the RBC skeleton was approximated by two concentric circles. Such geometry emphasizes that the discoid shape involves two rather flat sides, but neglects the part of the membrane at the cell rim, by which they are connected. In the second case the resting shape of the cell is taken to be a biconcave shape [11]. In the third case the RBC in its resting state is approximated by a sphere. The first and third geometries represent two opposing limits of the possible shape of the initial state of the skeleton. The reference biconcave discoid represents a generally used shape which was determined by Evans and Fung [11].

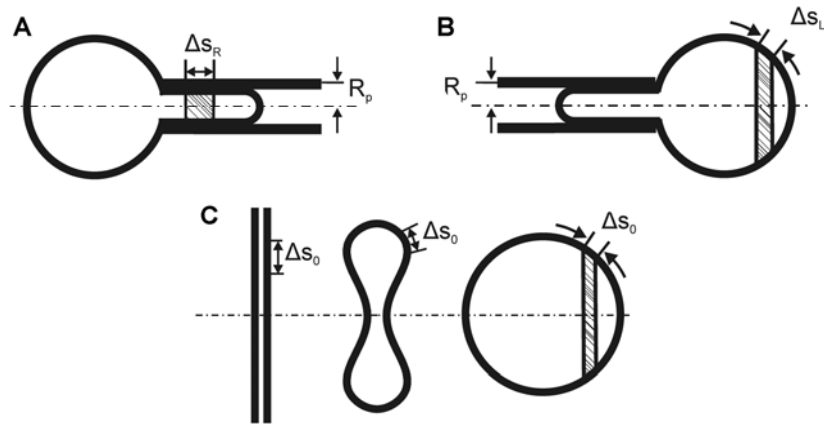


Fig. 1. Schematic representation of the method used to measure the RBC skeleton deformation [10]. A – RBC aspirated into the right micropipette. The labeled interval is Δs_R . B – RBC aspirated into a micropipette positioned to the left. The labeled interval from the first aspiration is transformed into the interval Δs_L . C – Initial geometries of the skeleton: two circles, biconcave shape and a sphere. Δs_0 is the interval on the initial geometry that transforms into the labeled intervals on the deformed cells in (A) and (B).

For all of the considered skeleton initial shapes we simulated skeleton redistribution for a simple deformation – the aspiration of the RBC into a micropipette. In the following section we shall outline the theoretical approach used to model the skeleton deformation. In the Results we shall present the behavior of the skeleton in all simulations and evaluate the differences between the initial shapes used.

THEORY

In this section we shall define the skeleton deformation and indicate the method for determination of the corresponding elastic energy. The RBC's skeleton is a quasi-triangular, two-dimensional network built from bonds and nodes. The bonds are spectrin tetramers and the nodes are junctional complexes based on short actin filaments [12]. It can be assumed that the skeleton elasticity depends mainly on the elasticity of the bonds. The deformation of the skeleton network is treated here by a recently developed continuum model of spectrin elasticity [Svetina, S. *et al.* The response of red blood cell membrane skeleton to deformations caused by geometrical constrains, in preparation]. In the applied procedure it is assumed that a finite rectangular patch of the skeleton with an area of $a \times b$ contains a sufficient number of bonds that are in the resting state oriented randomly in all directions within the plane of the membrane. The deformation of the patch is described in terms of two extension ratios, λ_1 and λ_2 , meaning that the deformed rectangle has the area $\lambda_1 a \times \lambda_2 b$. For a bond whose direction is defined by the angle φ we determine the energy of deformation by describing the elastic properties of the spectrin bonds in terms of Hookean springs. The energy of a bond is then proportional to the square of the difference

between the length of the bond in the deformed state and the bond's equilibrium length and described in terms of extension ratios λ_1 and λ_2 , and angle φ . The energy of a single bond averaged over all bond orientations depends on the elastic constant of the Hookean spring k and the extension ratios λ_1 and λ_2 . The area density of the skeleton energy is the product of the average bond energy and the area density of the undeformed bonds. It depends on the change of the skeleton area and its shear deformation. The total energy of the skeleton is then the integral of the area density of the skeleton energy over the area of the undeformed skeleton.

The deformations are determined for a cylindrical geometry; therefore, we define λ_1 and λ_2 as the extension ratios along meridians (λ_m) and parallels (λ_p), as

$$\lambda_m = \frac{ds}{ds_0}, \quad (1)$$

$$\lambda_p = \frac{r(s)}{r_0(s_0)}. \quad (2)$$

The parameters s and s_0 are the arc lengths measured from one of the cell poles, and r and r_0 are the distances from the axis (Fig. 2). The functions $r(s)$ and $r_0(s_0)$ are thus the contours of the deformed and undeformed shapes of the skeleton, respectively. The reduced skeleton density ρ can be expressed as

$$\rho = \frac{1}{\lambda_m \lambda_p}. \quad (3)$$

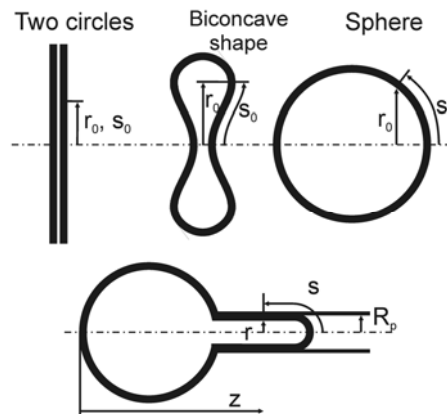


Fig. 2. Definition of the geometrical parameters used to define the skeleton deformation. The first model simulates the shape of the RBC membrane as two concentric circles, the second model as a biconcave disc and the third model as a sphere. The contour of the axisymmetric shape of the skeleton is given on the undeformed cell by the distance from the axis r_0 and the arc length s_0 , which is measured from the right pole. The corresponding contour of the deformed cell is given by r and s . R_p is the micropipette radius. The coordinate z is the distance from the left pole.

The skeleton at position s_0 moves to the unknown position s on the deformed shape. The mapping function, which defines from which point on the undeformed surface the bond reached the point s , is introduced as $s_0(s)$ [13, 14] and it is derived by variational calculation. It is to be pointed out that because spring constant k appears in the expression of the skeleton energy as a constant factor, the variationally obtained mapping function does not depend on its magnitude and therefore also not on the corresponding extension and shear moduli. In the calculation procedure, the skeleton redistributions obtained for each geometrical part of the deformed cell separately are combined by the requirements that the extension ratios λ_m and λ_p are equal at the poles and continuous from one geometrical part to another. The amount of the skeleton and its total area are conserved. Different projection lengths (L/R_p) were obtained by adjusting the volume of the RBC.

RESULTS

The simulation of the deformation of the RBC aspirated into the micropipette was first performed for three initial geometries (two concentric circles, a biconcave shape and a sphere) for the stress-free initial skeleton distribution (Figs. 1 and 2). The total area of the initial skeleton was taken to be the same for all models ($A_0 = 134.1 \mu\text{m}^2$). The pipette radius used was $R_p = 1.30 \mu\text{m}$. The length of the aspirated part of the cell was $1.69 \mu\text{m}$ and to get a spherical outside cell shape we made calculations for a cell volume of $138.7 \mu\text{m}^3$.

The skeleton redistribution, defined by the extension ratios λ_m and λ_p and the reduced skeleton lateral density ρ , was obtained for all models (Fig. 3). The dependences of λ_m , λ_p and $1/\lambda_m\lambda_p$ on the coordinate z along the aspirated cell are shown. The results obtained for each model differ in several aspects. A notable difference between the obtained lateral distributions is in the behavior of the skeleton at the external spherical part of the aspirated cell. In the spherical case the corresponding extension ratios and the skeleton density do not vary appreciably, which is understood to be because the radius of the sphere of the aspirated cell does not differ very much from the radius of the initial sphere. In contrast to this, in the case of the two circles and in the case of the biconcave shape the extension ratio λ_p has a minimum, whereas λ_m goes through a maximum. In the case of two circles these extremes are sharp-edged because of the discontinuous connection between the two circles. The second evident difference between the models is in the skeleton extension ratios at the hemispherical cap within the aspirated part of the cell. The skeleton there is more extended in the case of the two circles than in the case of the sphere. The extension ratios in the cell pole are 2.86 for the two circles, 2.25 for the biconcave shape and 2.02 for the sphere. The skeleton density is also different;

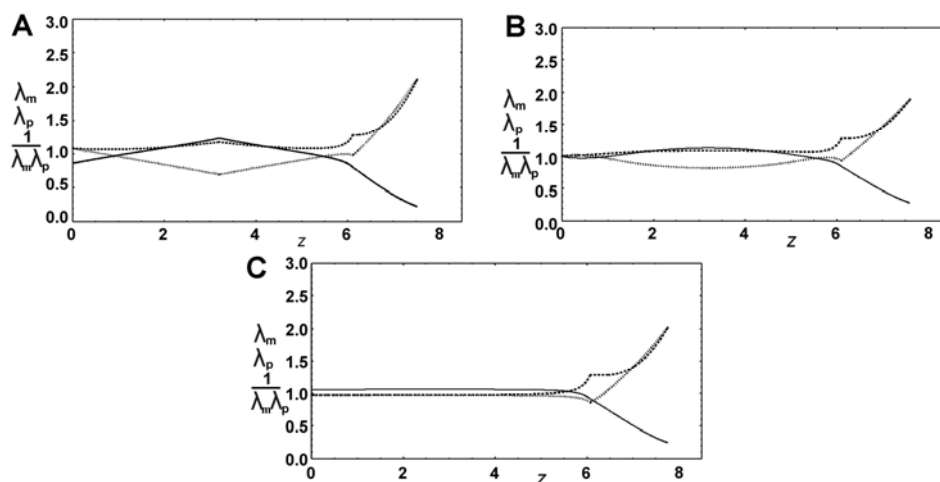


Fig. 3. The dependence of the extension ratios and the reduced density on the coordinate z for the stress-free initial state (A – two circles, B – biconcave shape, C – sphere) as obtained by the variational calculus described in Theory. The diagrams show extensions along the meridians (λ_m , dashed line), along the parallels (λ_p , dotted line) and the reduced density ($\rho=1/\lambda_m\lambda_p$, full line) of the skeleton distribution. The part of the curves where z is between 0 and approx. 6 corresponds to the outer part of the aspirated cell; the part between 6 and 6.5 corresponds to the cylindrical part of the cell in the micropipette; and the rest (6.5-8) corresponds to the semi-spherical cap of the deformed cell.

its pole value in the case of the two circles is 0.12, whereas the corresponding value in the case of the biconcave shape is 0.20 and in the case of the sphere is 0.26. The differences in the skeleton behavior in the hemispherical cap can be understood in terms of the different relative fractions of the skeleton in different parts of the micropipette, presented in Table 1. In the case of the two circles, more skeleton at the hemispherical cap is dragged out of the corresponding region than in the case of the biconcave shape, where there is also more skeleton dragged out of this region than in the case of a sphere, so in the first case there is the largest extension in the cell pole and in the third case there is the smallest.

The “two-micropipette approach” described in Fig. 1 was then simulated for each geometrical model of the resting shape of the RBC. The skeleton network was labeled in the middle of the cylindrical part when the cell was aspirated into

Table 1. The amount of skeleton in different parts of the aspirated cell relative to its initial amount in these parts.

Initial geometry	Relative fractions		
	External part	Cylinder	Hemispherical cap
Two circles	1.067	0.721	0.329
Biconcave shape	1.058	0.765	0.409
Sphere	1.051	0.829	0.474

a micropipette from the right (Fig. 1A). We then determined how the labeled part moved in the cell that was aspirated from the left-hand side (Fig 1B). The extension ratios along the meridians λ_m^{Lee} were defined by Lee *et al.* [10] as the ratio between the widths of the labeled section

$$\lambda_m^{\text{Lee}} = \frac{\Delta S_R}{\Delta S_L}, \quad (4)$$

where ΔS_R is the width of the marked interval of the skeleton when the cell is aspirated from the right and ΔS_L is the width of the interval when the cell is aspirated from the left. The extension ratios by Lee *et al.* [10] were obtained by considering that the radius of the outer spherical part of the aspirated cell does not differ appreciably from the radius of the initial sphere. So the outer spherical part of the “left” aspirated RBC is taken as an approximation of the stress-free state. In contrast to this approximation we obtained the extension ratios by considering the two treated limits of the initial skeleton geometry. The extension ratio along the meridians λ_m is calculated using the width of the labeled interval in the case of aspiration, and in the case of the undeformed cell

$$\lambda_m = \frac{\Delta S_R}{\Delta S_0}, \quad (5)$$

where ΔS_R is the same as before, but ΔS_0 is the labeled interval on the initial geometry of the undeformed cell (Fig. 1). The values of the extension ratios are presented in Table 2.

Table 2. Extension ratios along the meridians obtained by the method of Lee *et al.* [10] and by assuming three different resting states of the skeleton with unstressed bonds (for details see text).

Initial geometry	Extension ratios	
	λ_m^{Lee}	λ_m
Two circles	1.213	1.284
Biconcave shape	1.285	1.286
Sphere	1.316	1.280

All the calculations were performed also by assuming that the skeleton in the resting state of the RBC is uniformly stressed. We simulated the prestress model of Discher *et al.* [2], where the junctions on the skeleton are forced to be either closer together or more distant in the cell than they would be if the skeleton were separated from its bilayer. The spectrin bond that is connecting two junctions with its equilibrium length $L_{0,0}$ was stressed (condensed or stretched) to length L_0 , which is the initial length of the bond. The ‘prestress factor’ is defined as the ratio between lengths $L_{0,0}/L_0$. When the ratio is smaller than 1, the bond in its initial state is extended and when it is larger than 1, the bond in its initial state is compressed. Skeleton deformation was tested for the prestress factors from

0.8 to 1.7. The extension ratios at the hemispherical cap obtained (not shown) were larger in the case of stretched bonds and smaller in the case of condensed bonds. The density at the cap was thus obtained to be higher at the condensed initial state of the bonds. The application of the prestress situation to the method of Lee *et al.* [10] shows that the prestressed skeleton does not significantly affect the results presented in Table 2.

DISCUSSION

The RBC skeleton is a two-dimensional network whose macroscopic elastic properties exhibit shear elasticity. It is laterally much softer than the lipid bilayer part of the RBC membrane. RBC deformations cause large extensions of the spectrin tetramers, which are the prevailing microscopic, elastic element of the RBC membrane [2]. It is expected that the skeleton deformation depends on the initial state of the network and on how the system changes its geometry. A possible assumption is that when the cell is in its resting shape, e.g., the discocyte, the skeleton elements are distributed uniformly and are in the initial stress-free state. But it can also be assumed that the skeleton is distributed uniformly and in a stress-free manner when the RBC is spherical. It is also possible that the real RBC, whether it is in a biconcave or a spherical shape, is not at all in a stress-free distribution because of the variety of shapes assumed by the RBC during its passage through the blood [15].

A way to get some answers to the questions concerning the resting state of the skeleton is to measure its deformation under some well-defined experimental conditions and compare the obtained results with the predictions of calculations based on different assumptions about the initial skeleton lateral distribution. For this purpose we studied the effects on the skeleton lateral distribution in the case that the cell is aspirated into a micropipette with an aspiration pressure that causes the cell outside the micropipette to become spherical. The skeleton deformation and shape determination are then not coupled, as they are, for instance, when pulling a cell with two opposing beads attached to its membrane [16, 17]. The analysis of RBC aspiration is also of interest because it was possible on the basis of this method to measure the skeleton deformations directly [10].

We tested the effect of the initial state of the skeleton by choosing, as the initial skeleton geometry, two limiting cases, i.e., two flat circles and a sphere, and the intermediate biconcave shape (Figs. 1 and 2). The first of these initial geometries is an approximation to the discocytic RBC in that it emphasizes the two flat sides of the RBC discoid geometry. The biconcave shape presents the generally accepted shape of the resting state of the RBC and serves as a reference model. The spherical initial geometry, which is our third model, in an idealized way simulates the average of different shapes that the RBC experiences in the blood circulation.

The comparison of the results obtained for the three initial geometries (Fig. 3) shows why the deformational response differs for different changes of the

geometry. Different initial shapes of the RBC skeleton lead to different skeleton distributions in the deformed state. The difference between the predictions of the models can be understood by comparing the geometrical changes involved. One of the geometrical parameters that matters is the length of the contour of the axial cross-section of the cell. Assuming the same initial area of the RBC membrane, the ratios between the contour lengths of either the two circles, the biconcave shape or the sphere and of the aspirated cell (which is the same in all cases) are 1.27, 1.21 and 1.14, respectively, for the models presented in Fig 3. With the same deformation the skeleton is, therefore, more extended in the direction of its meridian in the cases of the two circles and the biconcave shape than in the case of the sphere. This is reflected in different distributions of the extension ratio λ_m . The effect of the change of the skeleton geometry on the extension ratio λ_p is due to the change of the distances of skeleton patches from the axis for different geometries. The course of the extension ratios at the spherical part outside the micropipette where the minimum of λ_p occurs is understood by larger distance of the skeleton close to the cell rim in the cases of two circles and the biconcave shape in comparison to the corresponding distance of the sphere of the aspirated cell. An important implication of our simulations is that a perturbation of the relatively small (aspirated) part of the membrane may have an effect on the skeleton density over the whole cell.

It was of interest to compare the numerical prediction of our three models and also their prestressed variations to the experimental data of Discher *et al.* [2]: densities of the skeleton near the pole of the hemispherical cap and at the micropipette entrance. Similarly as Discher *et al.* [3], we could obtain comparable results only by applying prestress (compressed) initial distribution of the skeleton. In our case the obtained densities for the prestress ratio $L_{0,0}/L_0$ between 1.3 and 1.7 better agreed at the entrance of the micropipette, whereas the densities at the pole of the hemispherical cap took too low values in comparison to the experimental and simulated data of Discher *et al.* [2, 3].

The simulations made were also used to evaluate the results of the “two micropipette approach.” Lee *et al.* [10] interpreted their results by using the sphere as the initial cell geometry. From Table 2 it can be seen that if we determine the extension ratio λ_m by the ratio between the widths of the bleached membrane section for the left and the right pipetting, the obtained result, in practice, depends on the initial geometry. However, the differences in the predictions of different initial skeleton geometries are not significant in view of possible experimental uncertainties. It is, however, necessary to keep in mind that the shifts from the correct values are systematic.

In conclusion, the presented analysis suggests that in studying deformations of the RBC membrane by observing the redistribution of its skeleton, the interpretation of the corresponding experimental results might depend on the choice of the RBC resting shape. The presented analysis also reveals that the skeleton redistribution caused by deformations is mainly the consequence of the change of the skeleton geometry.

Acknowledgement. This work was supported by the Slovenian Research Agency through grant P1-0055.

REFERENCES

1. Waugh, R.E. and Hochmuth, R.M. Mechanics and deformability of hematocytes. in: **The Biomedical Engineering Handbook** (Bronzino, J.D. Ed.), 2nd edition, CRC, Boca Raton, 1995, 474-486.
2. Discher, D.E. and Mohandas, N. Kinematics of red cell aspiration by fluorescence-imaged microdeformation. **Biophys. J.** 71 (1996) 1680-1694.
3. Discher, D.E., Boal, D.H. and Boey, S.K. Simulations of the erythrocyte cytoskeleton at large deformation. II. micropipette aspiration, **Biophys. J.** 75 (1998) 1584-1597.
4. Skalak, R., Tozeren, A., Zarda, R.P. and Chien, S. Strain energy function of red blood-cell membranes. **Biophys. J.** 13 (1973) 245-264.
5. Evans, E.A. New material concept for red-cell membrane. **Biophys. J.** 13 (1973a) 926-940.
6. Evans, E.A. New membrane concept applied to analysis of fluid shear-deformed and micropipet-deformed red blood-cells. **Biophys. J.** 13 (1973b) 941-954.
7. Brailsford, J.D., Korpman, R.A. and Bull, B.S. Red-cell shape from discocyte to hypotonic spherocyte - mathematical delineation based on a uniform shell hypothesis. **J. Theor. Biol.** 60 (1976) 131-145.
8. Fischer, T.M., Haest, C.W.M., Stohrliesen, M., Schmidtschonbein, H. and Skalak, R. The stress-free shape of the red-blood-cell membrane. **Biophys. J.** 34 (1981) 409-422.
9. Peng, Z., Asaro, R.J. and Zhu, Q. Multiscale simulation of erythrocyte membrane. **Phys. Rev. E.** 81 (2010) 031904.
10. Lee, J.C., Wong, D.T. and Discher, D.E. Direct measures of large, anisotropic strains in deformation of the erythrocyte cytoskeleton. **Biophys. J.** 77 (1999) 853-864.
11. Evans, E.A. and Fung, Y.C. Improved measurements of the erythrocyte geometry. **Microvasc. Res.** 4 (1972) 335-347.
12. Byers, T.J. and Branton, D. Visualization of the protein associations in the erythrocyte-membrane skeleton. **Proc. Natl. Acad. Sci. USA** 82 (1985) 6153-6157.
13. Mukhopadhyay, R., Lim, G. and Wortis, M. Echinocyte shapes: bending, stretching, and shear determine bump shape and spacing. **Biophys. J.** 82 (2002) 1756-1772.
14. Kuzman, D., Svetina, S., Waugh, R.E. and Žekš, B. Elastic properties of the red blood cell membrane that determine echinocyte deformability. **Eur. Biophys J.** 33 (2004) 1-15.
15. Fischer, T.M. Shape memory of human red blood cells. **Biophys. J.** 86 (2004) 3304-3313.

16. Henon, S., Guillaume, L., Richert, A. and Gallet, F. A new determination of the shear modulus of the human erythrocyte membrane using optical tweezers. **Biophys. J.** 86 (1999) 1145-1154.
17. Li, J., Dao, M., Lim, C.T. and Suresh, S. Spectrin-level modeling of the cytoskeleton and optical tweezers stretching of the erythrocyte. **Biophys. J.** 88 (2005) 3707-3719.